Heliyon

Received:
13 June 2018
Revised:
7 November 2018
Accepted:
21 January 2019

Cite as:
Ana María Carvajal-Bernal, Fernando Gómez-Granados, Liliana Giraldo, Juan Carlos Moreno-Piraján. Influence of stacked structure of carbons modified on its surface on n-pentane adsorption. Heliyon 5 (2019) e01156. doi: 10.1016/j.heliyon.2019.e01156

Influence of stacked structure of carbons modified on its surface on n-pentane adsorption

Ana María Carvajal-Bernal [a], **Fernando Gómez-Granados** [a], **Liliana Giraldo** [a], **Juan Carlos Moreno-Piraján** [b,*]

[a] *Departamento de Química, Facultad de Ciencias, Universidad Nacional de Colombia, Sede Bogotá, Colombia*

[b] *Laboratorio de Sólidos Porosos y Calorimetría, Departamento de Química, Facultad de Ciencias, Universidad de los Andes, Colombia*

* Corresponding author.
E-mail address: jumoreno@uniandes.edu.co (J.C. Moreno-Piraján).

Abstract

In this study, the microstructure of a series of activated carbons modified on its chemistry surface was evaluated from X-ray diffraction and porous structure analysis, and the effect of the stacked graphitic structure on the n-pentane adsorption capacity. The activated carbons were prepared modifying an activated carbon (obtained from coconut shell) by carbonization processes at 1073, 1173 and 1273 K and impregnation with 65% nitric acid solution, 60% phosphoric acid solution and reflux with 30% ammonium hydroxide solution. The activated carbons were characterized by N_2 adsorption at 77 K. It was found that these are essentially microporous materials with surface areas between 469 and 1113 $m^2\ g^{-1}$, and the evaluation of the microstructure was performed by determining the number of aromatic layers stacked from the analysis of the observed diffraction peak between 20-30° 2θ which corresponds to the 002 reflection in the plane of the coal using the STACK XRD technical. The results showed that impregnation as carbonization favours the development of the crystalline structure to the activated carbons, which is shown by the increase of the stacked structure at the same time; this favours the n-pentane adsorption.

https://doi.org/10.1016/j.heliyon.2019.e01156

Keyword: Physical chemistry

1. Introduction

The activated carbon is the most commonly used material in the industry for the removal of pollutants found in both the liquid phase (groundwater remediation, filtration of water for human consumption, adsorption of volatile organic compounds (VOCs), etc.), and the gas phase (air).

The adsorption capacity of an activated carbon is related to its porous structure and chemical surface. An activated carbon possesses micropores ($Ø < 2$ nm), mesopores ($2 < Ø < 50$ nm), and macropores ($Ø > 50$ nm) in different proportions, as defined by the IUPAC [1, 2]. The micropores play an important role in the adsorption of small adsorbate molecules, while macropores and mesopores are necessary in the transport of the adsorbate toward the micropores.

The porosity of the activated carbon is due to its microtexture, which results from stacking the aromatic layers that are responsible for lots of the crystalline structure, along with aliphatic chains and heteroatoms in the periphery that contribute to the amorphous structure of [3].

The microtexture of an activated carbon can be assessed by X-ray diffraction; this is a non-destructive technique that provides useful information for structural characterization from the determination of the fraction stacking structure [4, 5, 6, 7]. It has been made using the Gakushin's specification for the calculation of the cross-linkage constants and crystalline sizes of carbonaceous materials [8]. The Committee of the Japan Society for the Promotion of Science developed this method in 1963 [9]. Then, the activated carbon diffractograms are examined by Fourier analysis, to determine the number of aromatic layers that make up the stacks. The aromatic fraction of the stacked structure is equivalent to the fraction of the crystalline structure; this technique is called Stack-XRD (Standard analysis of coal by XRD) and it was developed by Hirch and Diamond [3, 5].

The VOCs, within which class is n-pentane, come from the solvents used as constituents in the formulation of resins, pigments, paints, oils, dyes, cosmetics, toiletries and cleaning products; this is part of the hydrocarbons that make up the gasoline among many others [10, 11]. Within the VOCs are alkanes, alkenes, alcohols, aldehydes, ethers and carboxylic acids; when they are broken down into reagents, these are combined with other impurities in the atmosphere to produce ozone, which is a precursor to the formation of photochemical smog. Ozone has been classified as a "Criteria Pollutant" by the Environmental Protection Agency (EPA) [12, 13].

https://doi.org/10.1016/j.heliyon.2019.e01156

In this study, an activated carbon produced from coconut shell was modified by impregnation at a moderate temperature of 291 K with a solution of nitric acid to 65% and a solution of phosphoric acid to 85%; these modify the surface chemistry and the porous structure of the activated carbon through the increased number of acid groups and the cross-linking of phosphate groups, respectively. The activated carbon treated with nitric acid was submitted to reflux in concentrated solution of ammonium hydroxide in order to introduce nitrogen as a heteroatom in the carbonaceous structure through the formation of amide, amine pyridinic, pyrrolic and quaternary nitrogen groups [14, 15, 16]. Additionally, the original activated carbon is carbonized in nitrogen atmosphere at 1073, 1173 and 1273 K to reduce the oxygenated group content on the surface. From the Stack-XRD analysis, we want to determine how these treatments modify the crystalline structure of the activated carbon and at the same time how the changes in crystalline structure relate to the adsorption of n-pentane.

2. Materials and methods

2.1. Preparation of activated carbon samples

Different activated carbons were prepared by modifying an activated carbon from coconut shell. The treatments are described in Table 1.

In all cases, the relationship of activated carbon to impregnation agent was 1:3 p/p. The samples were impregnated at 291 K for 72 hours; then, they were washed with deionized water until a constant pH was reached and were finally dried in an oven at 378 K until a constant weight was achieved.

Table 1. Preparation of activated carbon samples.

Samples	Treatment
G	Granular activated carbon produced from coconut shell (original sample)
GN	G Impregnated with nitric solution of nitric acid to 60% (Nitric acid p. a. 65% Merck)
GNA	Reflux of the sample GN in concentrated solution of ammonium hydroxide solution for a period of 24 h (Ammonium hydroxide solution to 25% Merck)
GP	G Impregnated with solution of phosphoric acid to 60% (Ortho-phosphoric acid p.a. 85%)
GC_{1073}	Carbonization of G at 1073 K
GC_{1173}	Carbonization of G at 1173 K
GC_{1273}	Carbonization of G 1273 K

https://doi.org/10.1016/j.heliyon.2019.e01156

The carbonization of samples was performed in a horizontal oven at 5 °C min^{-1} for two hours in a nitrogen atmosphere.

2.2. Characterization of activated carbon samples

The adsorption of nitrogen, N_2, at 77 K was performed in a Quantachrome IQ; the respective isotherms were built and the values of B.E.T. surface area (S), micropore volume (V_o), total pore volume (V_T) and mesopore volume (V_{meso}), were determined [17]. Additionally the chemical parameters were evaluated by Boehm titration and pH in the point of zero charge and the analysis of samples for Raman spectroscopy and Elemental analysis [18].

2.3. Adsorption of n-pentane

The adsorption of n-pentane at 261.15 K on the activated carbons was performed in a sortometer built in the laboratory (Fig. 1), which operates based on the volumetric method. Initially, the samples of activated carbon were degassed up to 5.65 × 10^{-3} mbar. For the n-pentane adsorption, this was brought to the vapour phase heating in a balance tank at 343 K; subsequently, the n-pentane in the vapour phase was injected onto activated carbon in the sample holder by opening a valve that connects the balance tank and the cell with the sample. The amount of n-pentane adsorbed is determined from the difference between the initial pressure and the pressure balance obtained after each injection using Eq. (1). The n-pentane adsorption on activated carbons was carried out until the saturation pressure of the n-pentane at operating temperature.

$$n_{ads} = \frac{(P_e - P_i)V}{R^*T^*m} \tag{1}$$

where n_{ads} (μmol.g^{-1}) is the amount of n-pentane adsorbed, P_i and P_e (mbar) correspond to the pressure of the adsorbate injected initially and on the balance,

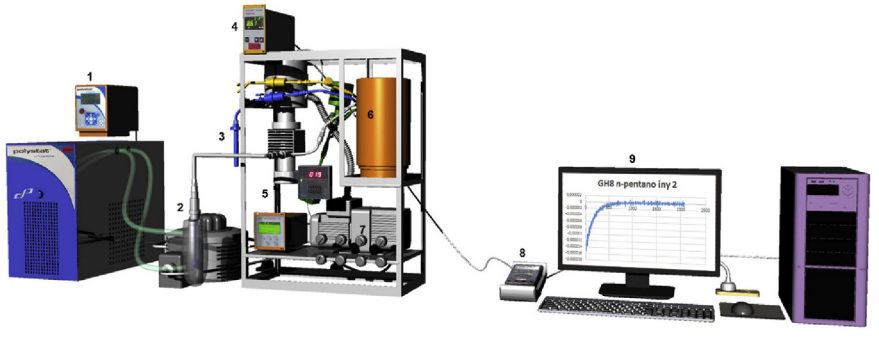

Fig. 1. Overview of the sortometer used for the n-pentane adsorption. 1. Thermostat, 2. Cell sample holder with activated carbon, 3. Solvent holder, 4. Pressure controller #1, 5. Pressure controller #2, 6. Equilibrium tank, 7. Control panel, 8. Voltmeter, 9. Data register. Diagram made by Luis Ariel Peña.

https://doi.org/10.1016/j.heliyon.2019.e01156

respectively, V (L) is the volume of the cell, R (mbar.L.μmol^{-1}.K^{-1}) is the gas constant, T (K) is the temperature of adsorption and m (g) is the mass of activated carbon.

2.4. X-ray diffraction

The X-rays diffraction patterns were determined in a XPERT-PRO diffractometer with CuKα radiation1, λ = 1.541874 Å with an acceleration electric potential of 45 kV and current applied of 40 mA with a range between 4 and 90°.

The activated carbon microstructure analysis was performed determining the number of aromatic layers stacked from the diffraction peak observed between 20° and 30° 2θ, which corresponds to the 002 reflection in c1c the plane of the coal. The intensity values were softened; subsequently, the correction of the widening of the intensity line due to the X-ray absorption phenomena, dispersion strengthened and structure were made by the Lorentz factor (L) Eq. (2), factor of polarization (P) Eq. (3), absorption factor (A) Eq. (4) and atomic scattering factor of coal (f) Eq. (6) [9], assuming that the sample consists only of structural carbon.

$$L = \frac{1}{1 + \sin^2 2\theta \cos^2 \theta} \tag{2}$$

$$P = \frac{1 + \cos 2\,\theta}{1 + \cos^2 2\theta} \tag{3}$$

The absorption factor (A) of the sample by x-ray diffraction is expressed as:

$$A = \left(1 + \frac{\sin 2\,\theta}{2\mu b_r}\right)\left(1 - \exp\left(\frac{-2\mu t}{\sin\theta}\right)\right) + \frac{2t\cos\theta}{b_r}\exp\frac{-2\mu t}{\sin\theta} \tag{4}$$

where μ is the coefficient of apparent absorption of the sample, μ = 10; t is the thickness of the sample in the sample holder equal to 0.2 mm; and b_r is the amplitude of the X-ray beam in the position of the sample and is expressed as:

$$b_r = R\sin\beta \tag{5}$$

where β and R correspond to the width of the grid of divergence, and the radius of the goniometer, respectively. The atomic scattering factor was calculated on the basis of:

$$\begin{aligned} f = {} & 2.26069\exp\left(-22.6907S^2\right) + 1.56165\exp\left(-656665S^2\right) \\ & + 1.05075\exp\left(-9.75618S^2\right) + 0.839259\exp\left(-55.5949S^2\right) + 0.286977 \end{aligned} \tag{6}$$

where s = sin θ/λ and the constants are the coefficients of Cromer-Man [19, 20], which for carbon is Z = 6.

https://doi.org/10.1016/j.heliyon.2019.e01156

Finally, the diffraction intensity smoothed is divided by the correction factor TCF = LPAf2 to obtain the intensity corrected (Icorr). The use of the graph of the intensity corrected as a function of the reciprocal distance $S = 2\sin\theta/\lambda$ has been suggested for the interpretation of peak 002, in order to obtain the true value of the maximum intensity [21]. The intensity of peak 002 (I_{002}) is obtained from:

$$I_{002} = \frac{S}{f^2}(I_{corr} - I_b) \tag{7}$$

where I_b is the intensity of a line that connects the minimum peak [3].

The Fourier transform method [4] was used to determine the distribution of the number of aromatic layers by stacking, N. The Fourier transform that has the form:

$$P(u) = 2\int_0^{\infty} \frac{I_{002}}{f^2}\cos 2\,\pi usds \tag{8}$$

is called "the Patterson function", which describes the probability of finding an aromatic layer at a normal distance to a layer [3, 22], therefore, this allows us to find the distribution of the stacks from the calculation of the second derivative of the weights of each peak in the Patterson function; that is to say, if p(n) is the weight of the nth peak in the function, then the probability f(n) of finding a stack with N layers ($N \geq 2$) is given by:

$$f(n) = \frac{P(n) - 2P(n+1) + P(n+2)}{P(1) - P(2)} \tag{9}$$

The relationship between the carbon atoms in a stack of layers aromatic and the total number of carbon atoms in the structure of the sample was determined from the fraction of stacked structure (Ps) [22], which is estimated from Eq. (10):

$$P_S(S) = \frac{SI}{SI(1 - I_{SP}) + I_{SP}} \tag{10}$$

where SI is the relationship between the intensity of peak 002 above the baseline and the total intensity. This parameter is calculated from:

$$SI = \frac{I_m - I_a}{I_m} \tag{11}$$

where I_m is the total intensity of peak 002 and Ia is the intensity below the baseline. I_{SP} represents the intensity generated by the crystalline component; that is to say, the aromatic layers stacked, which is equivalent to:

$$I_{SP} = \frac{0.0606}{S^2}\overline{N} \tag{12}$$

https://doi.org/10.1016/j.heliyon.2019.e01156

The average value $\breve{N}$ is estimated from the distribution of the number of aromatic layers by stacking (N), using Eq. (13):

$$\overline{N} = \frac{\sum f(n)}{\sum \frac{f(n)}{n}} \tag{13}$$

3. Results and discussion

3.1. Textural analysis

Fig. 2 shows the adsorption isotherms of N_2 at 77 K for samples G, GN, GC_{1073} and GC_{1273}, and Table 2 shows the results obtained textural parameters calculated from nitrogen isotherms at 77 K. In this, it can be see that all of the activated carbons correspond to microporous solids according to the classification of the IUPAC [2] with a small hysteresis loop to relative pressures higher than 0.35, indicating that there are a low amount of macropores calculated for G at 0.020 cm^3g^{-1} due to the difference between the total pore volume and the micropore volume determined using the method of Dubinin-Radushkevich [23]; with respect to the activated carbons prepared from sample G, it can be observed that there are an increase in the mesoporosity of carbonized samples GC_{1073} and GC_{1273} with values of 0.066 and 0.068 cm^3g^{-1}, respectively.

It is noteworthy that in the case of the carbonized sample at 1073 K, GC_{1073} there was an increase both in the volume of micropores and in the apparent surface area

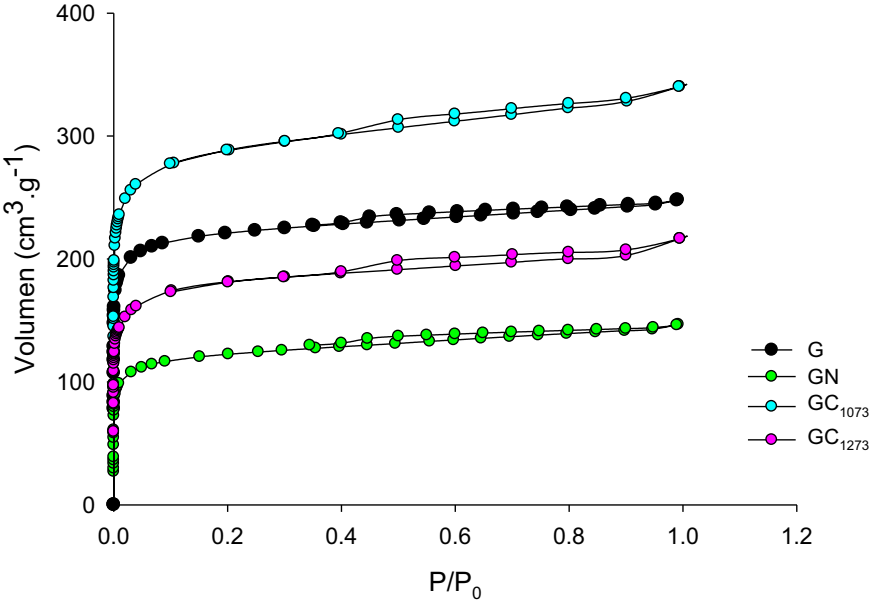

Fig. 2. Adsorption isotherms of nitrogen to 77 K. Some of the results have been presented above [15].

https://doi.org/10.1016/j.heliyon.2019.e01156

Table 2. Textural parameters from adsorption isotherm at 77 K[1].

Samples		G	GN	GNA	GP	GC_{1073}	GC_{1173}	GC_{1273}
S_{BET} (m^2g^{-1})		864	469	786	863	1113	813	708
C		1729	1149	1519	1287	1073	1130	898
DR Model	V_T (cm^3g^{-1})	0.38	0.22	0.34	0.39	0.51	0.36	0.31
	V_0 (cm^3g^{-1})	0.34	0.18	0.30	0.33	0.43	0.32	0.24
	Vmeso (cm3g-1)	0.04	0.04	0.04	0.06	0.08	0.04	0.07
	E ($kJmol^{-1}$)	25.8	22.2	26.7	24.1	24.6	25.0	27.7
QSDFT	V_T (cm^3g^{-1})	0.36	0.21	0.33	0.37	0.49	0.34	0.31
	Radio pore (Å)	6.0	10.1	7.6	8.0	6.8	8.0	11.9

1 V_0, micropore volume, Vmeso, both calculated from Dubinin Radushkevich (DR) method; V_T, total volume from, C, constant of the BET model.

S_{BET}, which indicates that carbonization allowed access to the microporous structure that was occluded, while carbonization at higher temperatures produces loss of both the surface area and the porous structure as evidenced by the values obtained for the GC_{1173} and GC_{1273} adsorbents.

Fig. 3 shows the change of the surface areas B.E.T. calculated from the adsorption isotherms of nitrogen to 77 K for the activated carbon samples, using the model of Brunauer, Emmett, Teller and Elovich [23, 24]. In relation to the micropore volume also determined from the isotherms of nitrogen to 77 K, the Dubinin-Raduskevich model was used in the range of P/P^0 between 1×10^{-5} and 0.1 from the expression:

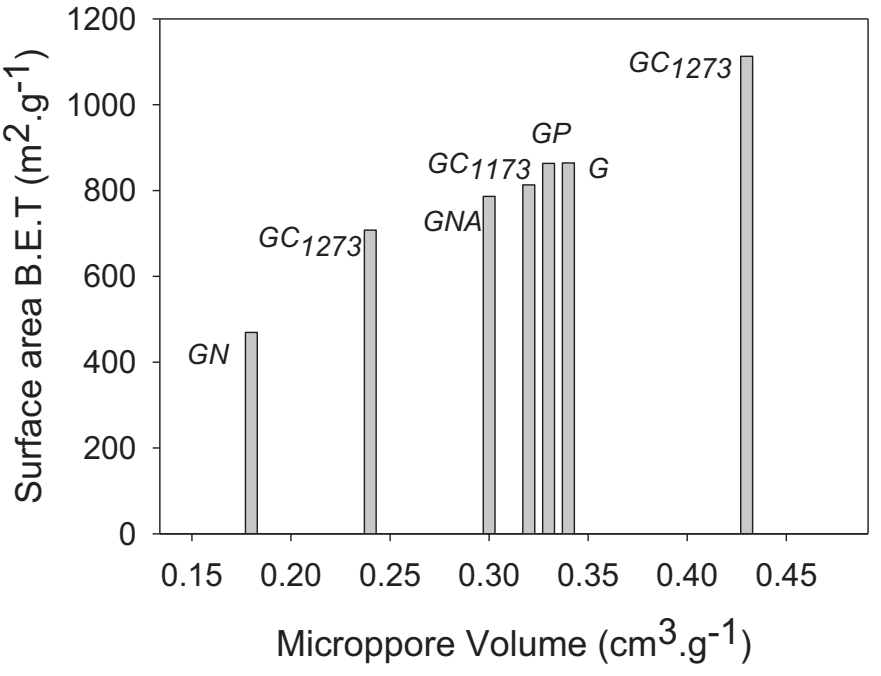

Fig. 3. Relationship between the B.E.T. area and micropore volume for the samples in the study.

https://doi.org/10.1016/j.heliyon.2019.e01156

$$\ln V = \ln V_0 - \frac{RT}{E}\ln\left(\frac{P^o}{P_e}\right)^2 \quad (14a)$$

where V is the volume of N_2 adsorbed in liquid phase to the equilibrium pressure P_e and V_0 is the micropore volume [23, 25].

In Fig. 3, it can be seen that in all cases, there are modifications of the surface area and micropore volume of the original activated carbon G. In the impregnation with nitric acid, there is a decrease in surface area in 45%, which is associated with the oxidation of this, and in the carbonization to 1073 K there is an increase of surface area of 28% that is attributable to opening of the structure occluded in the sample, while the carbonization at higher temperatures of 1173 and 1273 K shows a loss of surface area. As for the GNA and GN samples, it is noteworthy that in the case of GNA there is a recovery of the surface area by 40% with respect to the activated carbon GN with which it was prepared; this could indicate that the treatment of GN samples with ammonium hydroxide also generates nitrogen on the surface of the activated carbon, and reacts with the nitric acid that was obstructing the porosity of the GN sample or huge amount of surface oxygen groups (especially carboxylic acids) in the entrance of the pores that impedes the access to the porosity [18, 26, 27]. With regard to GP, the treatment of G sample with phosphoric acid produced only a loss of surface of 9%. This result is interesting because it suggests that although the nitric acid is a strong oxidant, the impregnation of the activated carbon with this agent to 291 K allows it to develop the surface chemistry of this without significantly affecting the microporous structure.

The evaluation of the total pore volume determined by the Quenched Solid Density Functional Theory (QSDFT) was carried out on the adsorption branch, assuming a pore structure composed of slits and cylinders; this presented values with errors less than 0.029% in general. In the distribution of the average width of the pore (Fig. 4), it can be observed that the pores are the pores are grouped into three zones: the first between 3 and 8 Å, the second between 10 and 20 Å. And the third between 20 and 50 Å. These results are interesting because they show that the carbonization to 1273 K destroyed the microporous structure in the range from 3 to 8 Å, while the treatment to 1073 K increased the porosity in these ranges in addition to that found between 20 and 50 Å. In regard to the impregnation with nitric acid, this decreased the pores between 3 and 8 Å. In general, analysis of the distribution of pores allows us to observe that all of the treatments modified the porosity of the initial activated G and new pores are generated this way.

3.2. Chemical characterisation

Table 3 shows the results obtained for chemical characterization by Boehm titration and pH in the point zero of charge, pH_{PZC} for activated carbon samples.

https://doi.org/10.1016/j.heliyon.2019.e01156

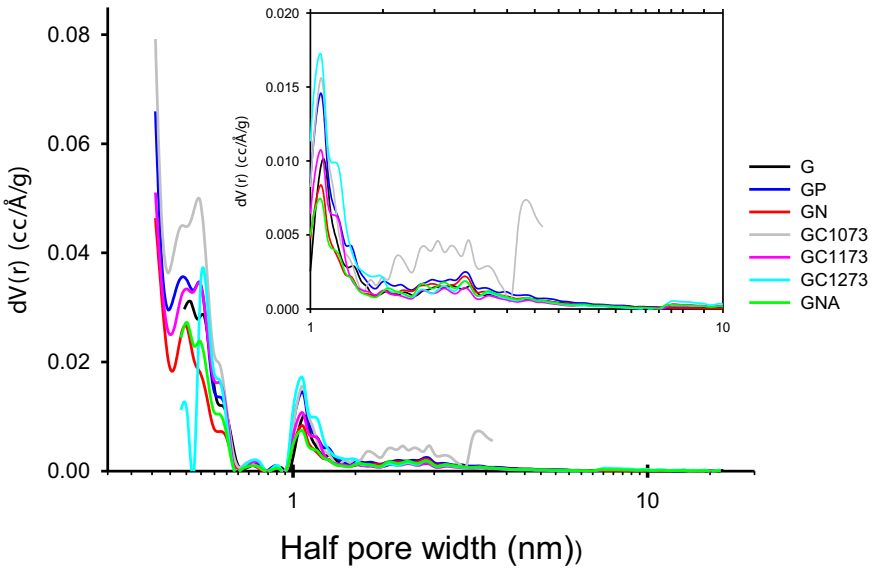

Fig. 4. Pore size distribution. (QSDFT method slit/cylinder. Pores, adsorption branch).

Table 3. Chemical parameters of the activated carbons.

Samples	Total Acidity ($\mu molg^{-1}$)	Total Basicity ($\mu molg^{-1}$)	Carboxylic Groups ($\mu molg^{-1}$)	Lactonic Groups ($\mu molg^{-1}$)	Phenolic Groups ($\mu molg^{-1}$)	pH_{PZC}
G	90.5	742	22.2	21.8	46.6	7.48
GN	6560	735	106	489.5	59.9	3.13
GNA	377	799	63.2	289	24.6	7.41
GP	423	849	109	137	177	5.91
GC_{1073}	93.6	1210	66.1	21.2	6.36	7.65
GC_{1173}	93.0	1630	65.5	23.8	3.71	7.89
GC_{1273}	94.1	2040	64.7	46.8	17.5	9.97

In Table 3, it can be see that all the treatments carried out modified the surface chemistry of the starting activated carbon G; in the case of the total acidity produced by some oxygenated groups in the periphery of the graphene layers of activated carbon, it is observed that the impregnations with nitric acid and phosphoric acid increased the content of acid groups of activated carbon G, the functionalization of the pre-oxidized sample GN with ammonium hydroxide reduced the content of the acid groups in the oxidized sample by 42%, which can be associated with the formation of nitrogenous groups from the acid groups produced in the sample GN; in the same way this increase in the content of acidic groups, is reflected in the values obtained for the pH_{PZC} of these samples.

Regarding the impregnation with H_3PO_4, in Table 3 it is observed that for this sample there is an increase in the content of phenolic groups of 3 times in relation to the

https://doi.org/10.1016/j.heliyon.2019.e01156

original sample G which can be attributed to the OH groups in the esters phosphocarbonaceous and pyrophosphate species that possibly formed with the impregnation of sample G with H_3PO_4 at 291 K.

The basic sites on the surface of activated carbon arise from the presence of π-electrons, pyro-like structures and chromene-like structures, the results shown in Table 3 indicate that the carbonizations show an increase in the content of these groups in such a way that as the carbonization temperature of activated carbon increased, an increase in the content of basic groups was obtained that can be associated with the increase in graphitic structure.

3.3. Raman spectroscopy

In Table 4, the change in the intensity of bands D and G of the Raman spectra can be observed with the different treatments performed on activated carbon as well as the change in the intensity ratio between these bands. It has been reported that the relative intensity of the band D with respect to the relative intensity of the G band is associated with the inverse of the crystalline diameter along the basal plane determined by X-ray diffraction, that is, it can be associated with the degree of structural disorder [28, 29, 30, 31]. According to the results observed in Table 4 on the intensity of the D band for the different samples, this is in the order $GC_{1273} < GNA < GN < GC_{1173} < G < GP < GC_{1073}$, this indicates that the carbonization 1273 K produces an increase in the crystallinity of activated carbon.

Likewise, it is observed that the carbonized sample at 1073 K presents the highest content of discontinuous carbonaceous structure and that the carbonization at 1173 K presents more discontinuous structure than the original sample; this suggests that during carbonization the temperature increase allows a reorganization of the microporous structure passing through discontinuous structures towards a crystalline structure that is obtained as the temperature increases. Regarding the impregnations, it is observed that the GNA and GN samples increase the crystalline structure of the sample G.

Table 4. Ratio of the intensities of the D and G bands of the Raman spectra.

Sample	Band D	Band G	ID/IG
G	37.0703	41.7584	0.89
GN	30.597	33.3446	0.92
GNA	29.6345	31.4042	0.94
GP	38.5295	43.5281	0.89
GC_{1073}	45.7945	51.9419	0.88
GC_{1173}	34.1518	34.6486	0.99
GC_{1273}	23.6424	23.3164	1.01

https://doi.org/10.1016/j.heliyon.2019.e01156

3.4. X-ray analysis

The comparison between the diffraction profiles obtained for the activated carbon samples in the study is shown in Fig. 4. The band observed corresponds to the 002 reflection in the plane of the graphite obtained between 20° and 30° 2θ once the corrections to the intensity values are applied by softening the data and correcting the widening of the 002 band due to the phenomena of X-ray absorption, and strengthened dispersion and structure. In addition, the baseline was subtracted.

In Fig. 5, it is possible to observe the emergence of a peak at 29° 2θ ($2\text{sen}\theta/\lambda = 0.29$) toward the centre of reflection 002, which is accentuated in the order: G < GNA < GC_{1173} < GP < GN < GC_{1073} < GC_{1273}. It has been reported that the intensity of band 002 is associated with the structure of the stacked aromatic layers [5, 32]. These results indicate that: 1) carbonization at 1073 K favours the appearance of the stacked structure, 2) carbonization at 1173 K destroys the structure formed and 3) carbonization at 1273 K allows the formation of a new stacked structure.

Another interesting result is seen in the impregnation with phosphoric acid (GP) and nitric acid (GN), where it is also noted that the peak at 29° intensifies. In the impregnation with phosphoric acid, it has been found that this agent promotes the formation of phosphate and polyphosphate bonds that expand and crosslink the carbon matrix [33]; also, it was reported that the treatment of activated carbon with phosphoric compounds at 3273 K induces the development of graphitic crystallites; the results suggest that the crystalline structure and the area can also be increased by the

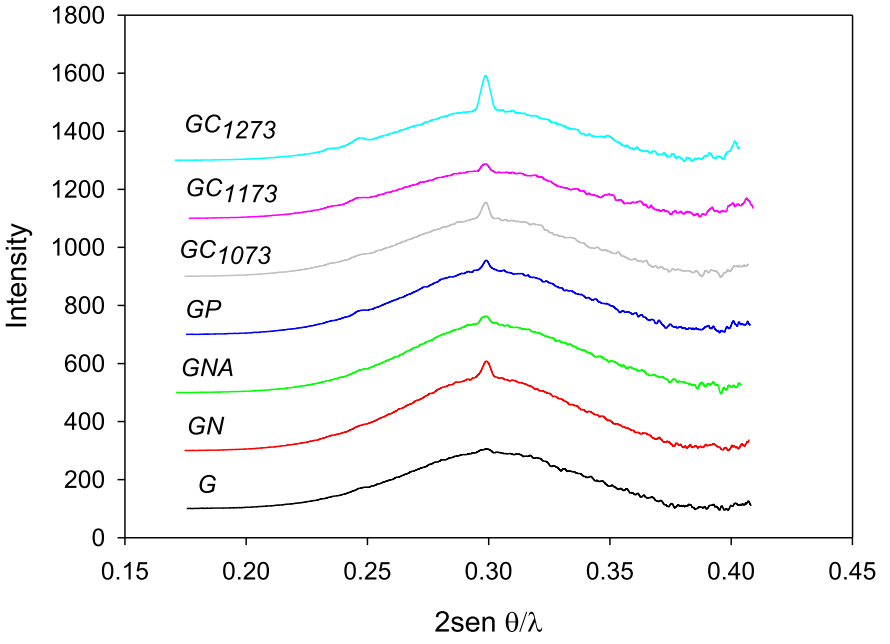

Fig. 5. Intensity of the 002 diffraction band in the plane of graphite (I_{002}) as a function of the reciprocal distance $S = 2\text{sen}\theta/\lambda$

https://doi.org/10.1016/j.heliyon.2019.e01156

treatment of activated carbon with phosphoric acid at 291 K. In regard to the impregnation with nitric acid, studies reported that the oxygen-containing functionalities are obtained by oxidation of the carbon [33], this treatment also destroys part of the microporous structure which could allow access to the occluded crystalline structure.

In Fig. 5, the widening of band 002 is further noted, which has been associated in other studies with the presence of amorphous structure in the activated carbon [5]; other studies report that in the analysis of a carbonaceous material by XRD, the widening of the 002 band can be attributed to coals and non-graphitic carbons, as resulting from structures made up of associations, roughly parallel, of hydrocarbon (polycyclic) moieties (for the macromolecular structure of coal) and of quite defective, non-planar but roughly parallel associations of carbon and termed the defective micro-graphene layers. That is, there is no planarity, only strain and defects [34].

The ratio of intensities of bands D and G in the Raman spectra for the activated carbon samples are compared with the fraction of the stacked structure (P_S) in Fig. 5.

In Fig. 6, it can be seen that as a general trend, the fraction of stacked structure Ps, increases with the fraction of crystalline structure; an interesting behavior is observed for the carbonized samples GC_{1073}, GC_{1173} and GC_{1273}, where the carbonization at 800°C of sample G produces an increase of the stacked structure, and this decreases with carbonization at 900°C while an increase in the crystalline structure occurs and finally, the carbonization at 1000°C generates again an increase of the

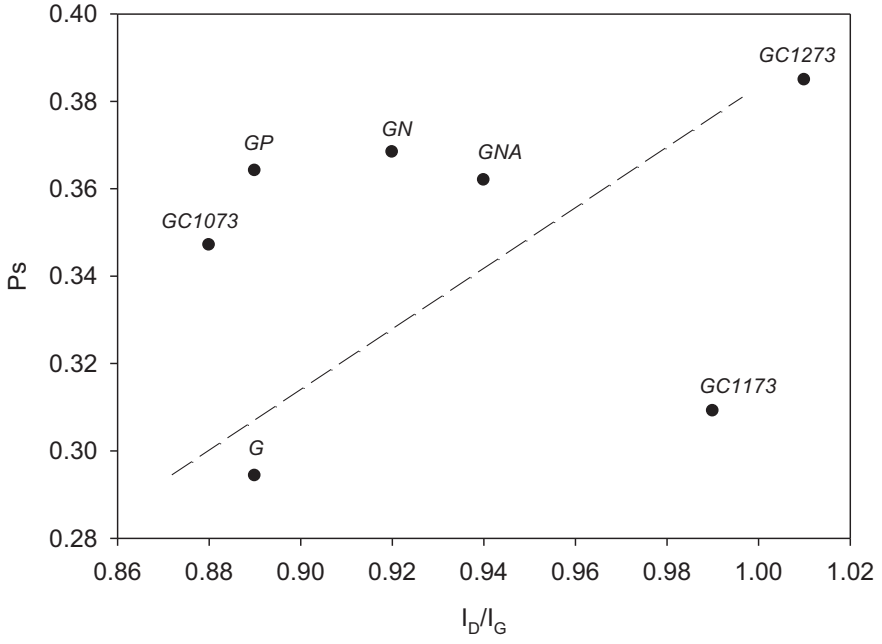

Fig. 6. Comparison between the ratio of intensities of bands D and G in the Raman spectra with the fraction of the stacked structure Ps.

https://doi.org/10.1016/j.heliyon.2019.e01156

stacked structure; these results are interesting because they show a reorganization of the crystalline structures which first passes through an amorphous structure. This suggests that, at an increased crystalline structure in the activated carbon, the amorphous structure decreases, which indicates that the crystalline structure is produced from amorphous structures during the carbonization processes.

Fig. 7 shows the function of Patterson and the distribution of the number of aromatic layers by stacking (N) to the carbons in the study.

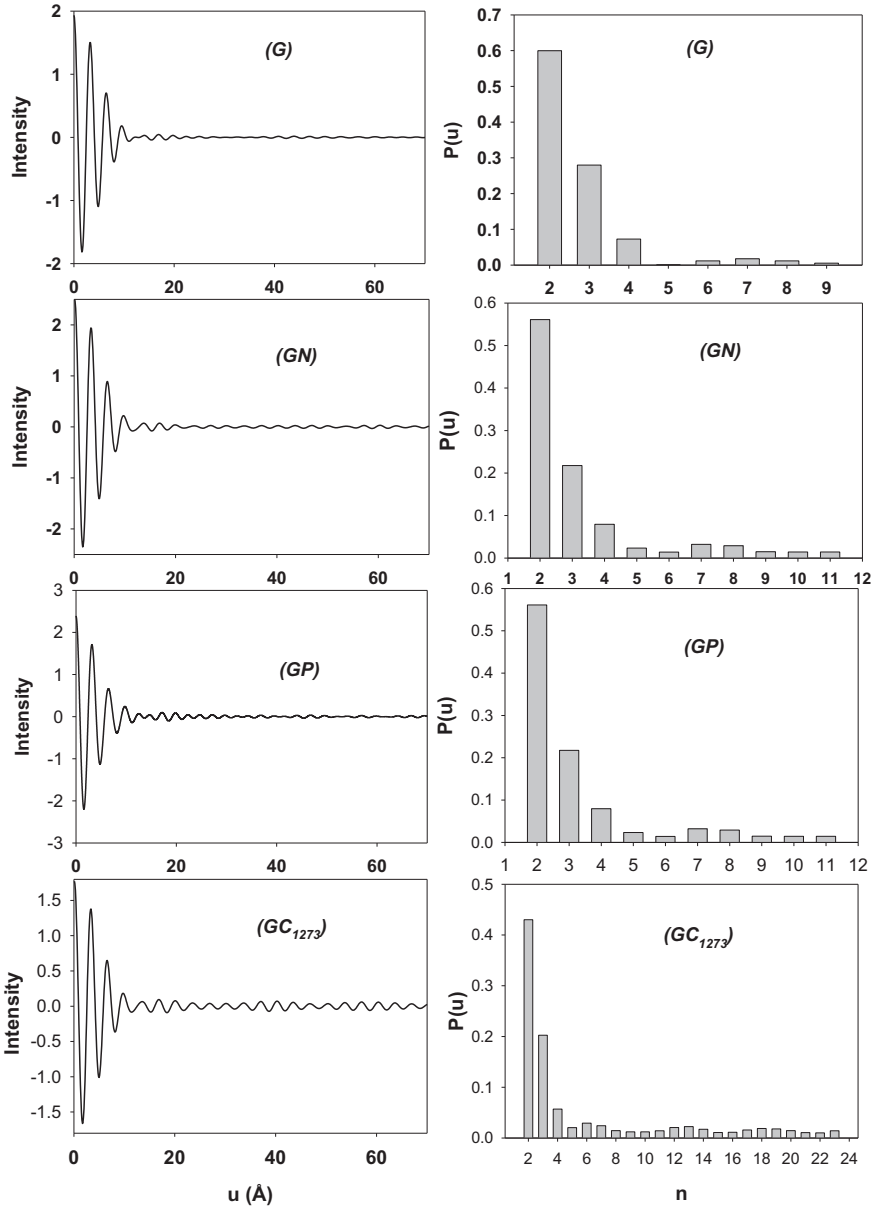

Fig. 7. Function of Patterson on the left and distribution of the number of aromatic layers by stacking (n) on the right to the carbons.

https://doi.org/10.1016/j.heliyon.2019.e01156

The Patterson model is a function that correlates the electron density evaluated at each point of a unit cell [35]; therefore, each peak in the function is associated with the probability that a stack is made up of N layers, for example, a value of P(u) of 0.6 for a stack N = 2 means that there is a 60% probability that the graphitic stacks contain 2 layers, taking this into account, the distribution of N estimated from Eq. (9) indicates that, on average, all samples of activated carbon are approximately 60% graphitic stacks of two layers, 25% stacks of 3 graphitic layers, about 30% graphitic stacks of 4 layers and less than 1% stacks of more than 4 layers.

An interesting result is observed for the sample impregnated with phosphoric acid GP) and the sample carbonized at 1273 K (GC_{1273}), is the increase of the probability of the existence of graphitic layers by stacking above 5 increases; in particular, for carbonized sample there is a 5% probability that small stacks (according to the calculation) of between 5 and 23 graphitic layers will be formed. These results are consistent with those presented to date and corroborate the formation of structures intertwined when activated carbon is treated with phosphoric acid and the formation of crystalline structures during carbonization.

Finally, the relationship between the fraction of stacked structure and the area BET for the carbons can be seen in Fig. 8. Here, it is possible to appreciate the decrease in surface area with the increase in the stacked structure as a general trend of the samples; this indicates that the crystalline structure formed does not contribute to the porosity of the activated carbons and, therefore, neither does the increase in the area.

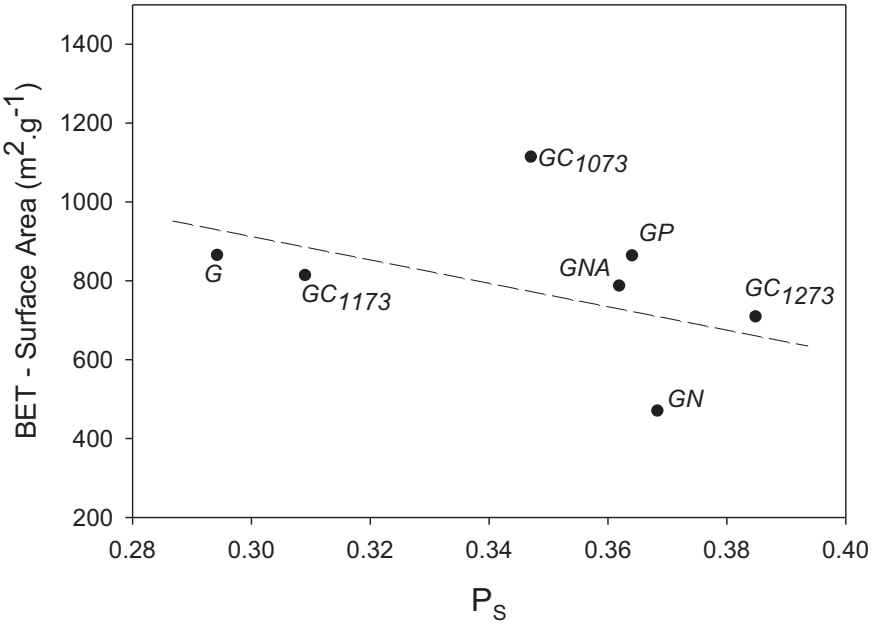

Fig. 8. BET surface area for the carbons in relation to the fraction of stacked structure.

https://doi.org/10.1016/j.heliyon.2019.e01156

3.5. Adsorption of n-pentane

The adsorption isotherms of n-pentane on different activated carbons at 261.15 K are presented in Fig. 9. Here, it is noted that the amount of n-pentane adsorbed increases proportionally with pressure at low relative pressure values of less than 0.1; at relative pressure values between 0.1 and 0.4, the isotherm is concave with respect to the axis of the relative pressure, indicating that the n-pentane monolayer adsorption reaches its maximum point, and above this pressure, the increase in adsorption is low compared to the increase in relative pressure. This behavior has been described by different models within which the Langmuir is one of the most commonly used. This implies that the maximum adsorption corresponds to a saturated monolayer of molecules of adsorbate that adsorb in defined places on the surface; in this, all sites are energetically equivalent. The adjustment of the data of the Langmuir adsorption model (Eq. 14a, b) [36], is summarized in Table 3, and the relationship between the fraction of structure stacked P_S and the maximum capacity of adsorption Qo n-pentane-determined by the Langmuir model is presented in Fig. 10.

In the Langmuir model, q_e ($\mu mol.g^{-1}$) is the amount of solute adsorbed per unit weight of the adsorbent in the balance, C_e ($\mu mol.L^{-1}$) is the concentration of solute in solution at equilibrium, Q_0 ($\mu mol.g^{-1}$) is the maximum capacity of adsorption and K_L is the Langmuir constant related to the free energy of adsorption ($L.\mu mol^{-1}$).

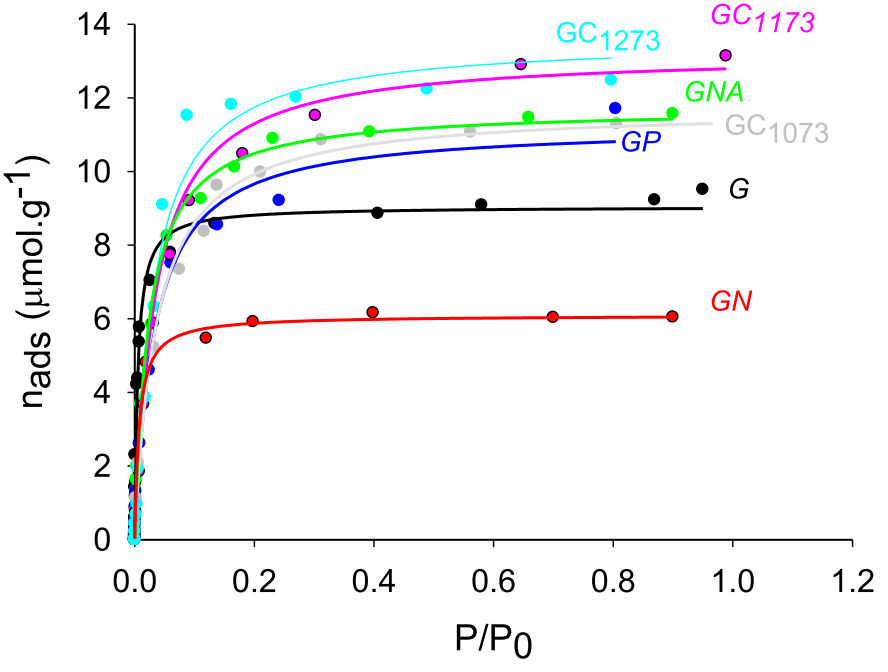

Fig. 9. Adsorption of n-pentane on activated carbons at 261 K. The lines correspond to the adjustment of the data to the Langmuir adsorption model.

https://doi.org/10.1016/j.heliyon.2019.e01156

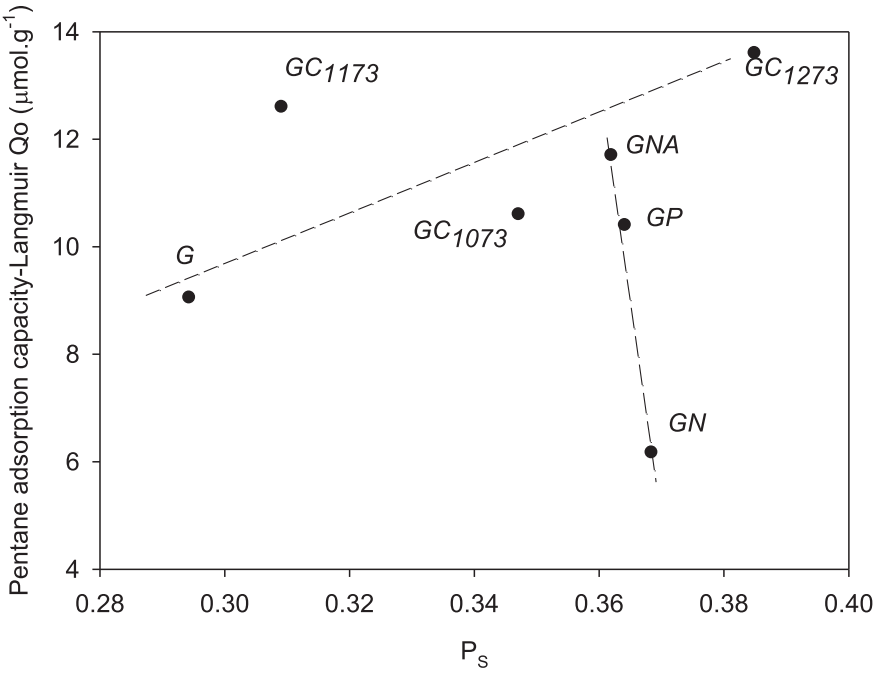

Fig. 10. Relationship between the fraction of stacked structure and the maximum capacity of adsorption Qo n-pentane, as determined by the Langmuir model.

$$q_e = \frac{Q_0 K_L C_e}{1 + K_L C_e} \tag{14b}$$

Table 5 shows that with the exception of impregnation with nitric acid, the other treatments favour the adsorption of n-pentane. For the impregnated samples, the maximum adsorption capacity Q_0 is increased in the order GN < GP < GNA; this behavior can be attributed to the oxygen groups in sample GN, phosphate groups in sample GP and nitrogen groups in sample GNA, as observed in Table 6 in which the results obtained for Elemental Analysis are shown. These groups make the n-pentane adopt a temporary dipole due to an excess of electrons on one side of the

Table 5. Adjustment of the n-pentane adsorption data to the Langmuir model.

Sample	Q_0	K_L	R
	$mmol.g^{-1}$	$L.\mu mol^{-1}$	
GN	6.2	130.9	0.9968
G	9.1	147.1	0.9838
GP	10.4	38.7	0.9978
GNA	10.5	52.7	0.9986
GC_{1073}	10.6	36.4	0.9978
GC_{1173}	12.6	27.4	0.9995
GC_{1273}	13.6	31.6	0.9939

https://doi.org/10.1016/j.heliyon.2019.e01156

Table 6. Elemental analysis.

Element	N (%)	C (%)	H (%)	O (%)
Retention time (min)	45	70	265	N.A.
G	0.22	69.88	0.47	29.43
GN	0.90	69.13	0.37	29.60
GNA	1.38	61.05	0.36	37.21
GP	0.31	69.00	0.53	29.83
GC_{1073}	0.33	81.20	0.63	17.84
GC_{1173}	0.24	78.46	0.44	20.85
GC_{1273}	0.27	77.74	0.36	21.64

molecule and, therefore, the adsorption in specific sites of the surface by ion-dipole interaction [37]; in additionally, in Table 6 it is possible to observe the increase in carbon content for the carbonized samples $GC_{1073} > GC_{1173} > GC_{1273}$ relative to the starting adsorbent G; this can be attributed to the increase in the graphitic structure caused by the carbonization process, these results are consistent with those obtained from X-ray diffraction analysis, in addition it is also observed that the carbon content decreases with the increase in the carbonization temperature, which can be attributed to the loss of surface groups.

With respect to the carbonized samples, the value of Q_0 increased in the order $GC_{1073} < GC_{1173} < GC_{1273}$; this behavior can be attributed to several phenomena: the destruction of the microporosity, increasing of the pore radius which would allow greater accessibility of the n-pentane to the microporous structure, increase in the stacked structure and increasing of basic groups.

With regard to the values for the constant K_L, these are between 27.4 and 147.1 $L.\mu mol^{-1}$, indicating that the adsorption of n-pentane is physical in all cases; higher values of K_L correspond to samples G and GN but at the same time these presented the lowest values in the maximum adsorption capacity Q_0 and in the stacks of aromatic layers. Taking into account that this constant is related to the energy produced by the interaction between the n-pentane and the surface, this would confirm that the adsorption of the n-pentane on these samples of activated carbon GN and G is performed at specific sites on the surface by Van der Waals forces resulting from the presence of oxygenated groups on the surface, as already described.

In Fig. 10 is possible to observe the negative correlation between the amount of surface oxygen groups per surface area of sample and the n-pentane adsorption capacity for GNA, GP and GN samples, positive correlations between carbonized samples; this indicate that Ps is related with clean carbon surfaces for heat treated carbons.

https://doi.org/10.1016/j.heliyon.2019.e01156

As mentioned above, since the process of the adsorption of n-pentane on the carbons in the study is physical in all cases, an equation that has been used to describe the physical adsorption of gases and vapours on microporous solids is the Dubinin Radushkevich model. This was used in the current study to evaluate the adsorption of the n-pentane on the microporous structure in the range of relative pressures between 1×10^{-5} and 0.1 using Eq. (14a, b). The adjustment results for the n-pentane adsorption isotherms on the activated carbon samples to the DR model are presented in Table 7. With comparative purposes, the immersion enthalpies of samples in n-pentane are also presented.

One aspect to highlight in the results shown in Table 7 is the values obtained for the micropore volume of activated carbon samples GNA and G, which indicate that the n-pentane agreed to a higher percentage with the porosity of the sample; the differences between the values of micopore volume from Tables 2 and 7 indicate that the n-pentane molecule does not access all the available microporosity in the adsorbents due to its larger size compared to the nitrogen molecule; in relation to the carbonized samples, a contrary tendency is observed in the micropore volume to which is presented in Table 2, this could be associated to the greater affinity of the n-pentane with a greater graphitic surface that is also evidenced in the higher values obtained for the enthalpy of immersion of the carbonized adsorbents compared with the starting adsorbent G.

The fraction of stacked structure (Ps) calculated with Eq. (11) for samples of activated carbon in relation with the characteristic energy for the adsorption of n-pentane calculated with the DR model are presented in Fig. 11. Here, it can be observed that for both carbonized and impregnated samples, there is an increase in the n-pentane adsorption energy as the fraction stacked structure increases; however, the GNA sample comes out of the trend by presenting the lowest value of characteristic energy and, at the same time, has one of the highest values in the

Table 7. Dubinin-Radushkevich model parameters obtained from the n-pentane adsorption isotherms at 261.15 K.

Sample	Vmicro	Adsorption Energy	n-pentane
	mm^3g^{-1}	KJ mol^{-1}	-ΔHimm, $J.g^{-1}$
GC_{1073}	1.30	15.14	74.5
GP	1.39	15.54	51.1
GC_{1173}	1.47	13.31	75.4
GN	1.49	15.28	39.6
GC_{1273}	1.79	12.95	73.8
GNA	3.38	10.03	44.9
G	4.14	11.41	70.6

https://doi.org/10.1016/j.heliyon.2019.e01156

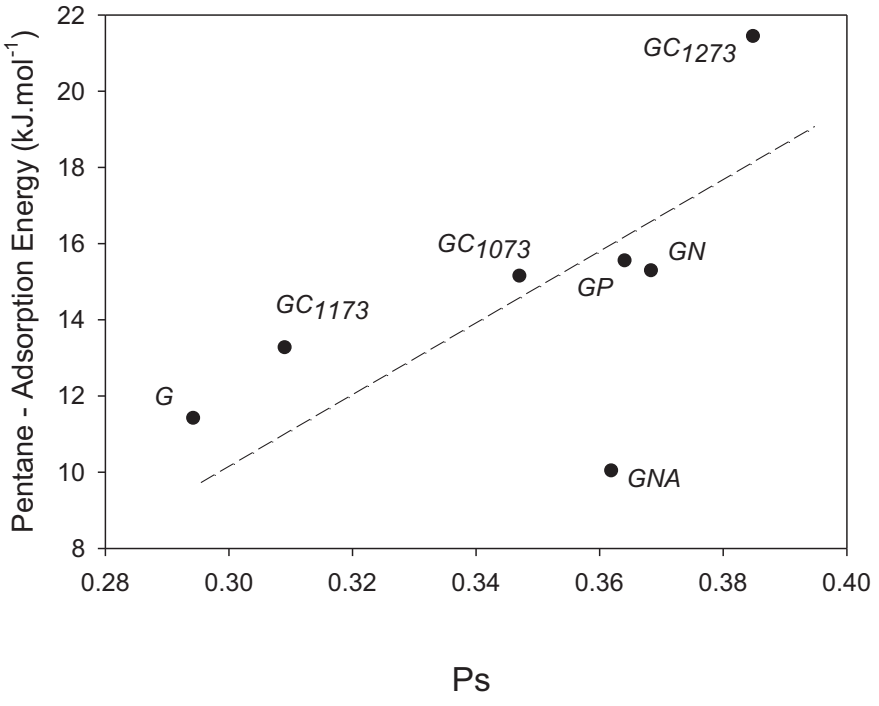

Fig. 11. The relationship between n-pentane adsorption energy and the fraction of stacked structure, PS.

fraction of stacked structure. This change in the trend could be attributed to the fact that this sample has the highest number of nitrogen groups on the surface, meaning that there are more interactions between the n-pentane and nitrogen groups in this sample than in others, possibly by an increase of permanent dipole-induced-dipole interactions.

As already mentioned, the increase in the value of Ps indicates the increase in the number of carbon atoms in a stack of aromatic layers in relation to the total number of carbon atoms in the structure; that is to say, this value increases with the increase in crystalline structure. The sample that presents the greatest fraction of stacked structure and at the same time the lower value of BET area is the sample carbonized at 1273 K. As noted in Fig. 3, the carbonization at this temperature resulted in the destruction of the microporosity between 0.4 and 0.5 nm; in addition, in Fig. 6, it was noted that the carbonization process at this temperature increased the number of aromatic layers by stacking. It is also important to note that the sample of initial activated carbon G is the one that presented the smallest fraction of stacked structure and one of the lowest values in the adsorption energy. These results suggest that the increase in the stacked structure could facilitate interactions between the n-pentane and the surface of the activated carbon.

Fig. 12 show the results of the scanning electron microscopy SEM analysis that was performed on the activated carbon sample G, GNA and GC_{1273}.

https://doi.org/10.1016/j.heliyon.2019.e01156

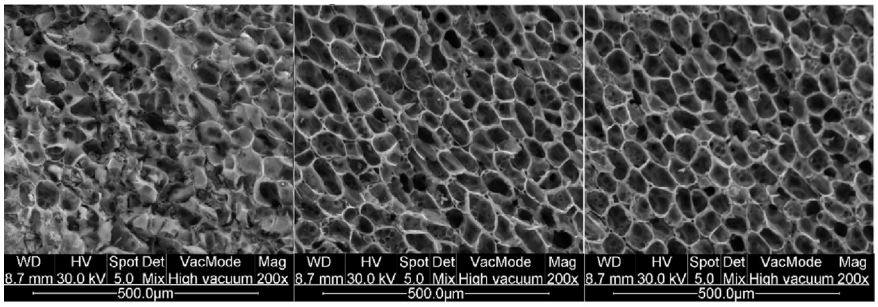

(a) (b) (c)

Fig. 12. Scanning electron microscopy SEM: GNA, G and GC_{1273} (a), (b) and (c) respectively.

The SEM images presented in Fig. 12 show that the modification made with HNO_3, and NH4OH have a corrosive effect on the activated carbon surface, which is evidenced in the appearance of amorphous structure for the GNA sample; with respect to the image of the carbonized sample GC1273 it is possible to observe that the carbonization favored the increase of ordered structure and this is consistent with the results obtained from the X-ray diffraction analysis shown above.

4. Conclusions

From textural parameters, Boehm titration, stakc XRD analysis, and n-pentane adsorption isotherms, it is possible to conclude that the impregnation of carbons to a moderate temperature of 291 K with concentrated solutions of nitric acid, phosphoric acid and reflux of preoxidized sample with a concentrated solution of ammonium hydroxide, as well as the carbonization temperatures of 1073, 1173 and 1273 K, modifies the amorphous structure, the crystalline structure, the porosity, the surface area and the n-pentane adsorption capacity of the activated carbons.

Impregnation with a solution of phosphoric acid at a moderate temperature of 291 K generates an increase in the number of aromatic layers by stacking N via cross-linking of the phosphate group on the activated carbon surface; therefore, there is an increase in the crystalline structure, the surface area and the capacity to adsorb n-pentane.

The GNA activated carbon prepared by reflux of the preoxidized sample in a concentrated solution of ammonium hydroxide presents nitrogen groups formed from the acid groups in the activated carbon pre-oxidezed GN. This favours the adsorption of n-pentane in the microporous structure because the nitrogen groups have a couple of unpaired electrons, which increases the possibility of altering the electron density of the molecule of n-pentane and generates a more induced ion-dipole interactions (Van der Waals) between the n-pentane and the surface of the activated carbon.

https://doi.org/10.1016/j.heliyon.2019.e01156

The relationship between the carbon atoms in a stack of aromatic layers and the total number of carbon atoms in the structure of the sample increases with carbonization; these facts favour the interaction between the surface of the activated carbon and n-pentane, which is reflected in the increase in energy of the adsorption calculated by the DR model.

The values of micropore volume of 3.38 mm^3g^{-1} for the GNA samples indicates that the access of the n-pentane to the microporous structure is favoured by the presence of nitrogen groups on the surface.

Declarations

Author contribution statement

Ana M. Carvajal-Bernal: Conceived and designed the experiments; Performed the experiments; Analyzed and interpreted the data; Wrote the paper.

Fernando Gómez Granados: Conceived and designed the experiments; Analyzed and interpreted the data.

Liliana Giraldo Gutiérrez, Juan Carlos Moreno Piraján: Conceived and designed the experiments; Analyzed and interpreted the data; Wrote the paper.

Funding statement

This work was supported by the Faculty of Sciences of Universidad de Los Andes through the call "short projects/additional product".

Competing interest statement

The authors declare no conflict of interest.

Additional information

No additional information is available for this paper.

References

[1] K.S. Sing, Reporting physisorption data for gas/solid systems with special reference to the determination of surface area and porosity (recommendations 1984), Pure Appl. Chem. 57 (1985) 603−619.

[2] M. Thommes, K. Kaneko, A.V. Neimark, J.P. Olivier, F. Rodriguez-Reinoso, J. Rouquerol, K.S. Sing, Physisorption of gases, with special reference to the

https://doi.org/10.1016/j.heliyon.2019.e01156

evaluation of surface area and pore size distribution (iupac technical report), Pure Appl. Chem. 87 (2015) 1051−1069.

[3] N. Yoshizawa, K. Maruyama, Y. Yamada, M. Zielinska-Blajet, Xrd evaluation of co 2 activation process of coal-and coconut shell-based carbons, Fuel 79 (2000) 1461−1466.

[4] P.B. Hirsch, X-ray scattering from coals, Proc. Roy. Soc. Lond. Math. Phys. Sci. 226 (1954) 143−169.

[5] D.P. Vargas Delgadillo, Preparación, caracterización y funcionalización de materiales carbonosos para la adsorción de co2, Universidad Nacional de Colombia, 2013.

[6] K. Krishnamoorthy, M. Veerapandian, K. Yun, S.-J. Kim, The chemical and structural analysis of graphene oxide with different degrees of oxidation, Carbon 53 (2013) 38−49.

[7] B. Manoj, A. Kunjomana, Study of stacking structure of amorphous carbon by x-ray diffraction technique, Int. J. Electrochem. Sci 7 (2012) 3127−3134. ISSN 1452-3981.

[8] K.S.W. Sing, F. Rouquerol, P. Llewellyn, J. Rouquerol, 9 - assessment of microporosity, in: F.R.R.S.W.S.L. Maurin (Ed.), Adsorption by Powders and Porous Solids, second ed., Academic Press, Oxford, 2014, pp. 303−320.

[9] N. Iwashita, C.R. Park, H. Fujimoto, M. Shiraishi, M. Inagaki, Specification for a standard procedure of x-ray diffraction measurements on carbon materials, Carbon 42 (2004) 701−714.

[10] G.Y. Gor, O. Paris, J. Prass, P.A. Russo, M.M.L. Ribeiro Carrott, A.V. Neimark, Adsorption of n-pentane on mesoporous silica and adsorbent deformation, Langmuir 29 (2013) 8601−8608.

[11] L. Zhang, G. Qian, Z. Liu, Q. Cui, H. Wang, H. Yao, Adsorption and separation properties of n-pentane/isopentane on zif-8, Separ. Purif. Technol. 156 (Part 2) (2015) 472−479.

[12] S. Subramanian, G. Pande, G. De Weireld, J.-M. Giraudon, J.-F. Lamonier, V.S. Batra, Sugarcane bagasse fly ash as an attractive agro-industry source for voc removal on porous carbon, Ind. Crop. Prod. 49 (2013) 108−116.

[13] R.R. Gil, B. Ruiz, M.S. Lozano, M.J. Martín, E. Fuente, Vocs removal by adsorption onto activated carbons from biocollagenic wastes of vegetable tanning, Chem. Eng. J. 245 (2014) 80−88.

https://doi.org/10.1016/j.heliyon.2019.e01156

[14] R. Jansen, H. Van Bekkum, Amination and ammoxidation of activated carbons, Carbon 32 (1994) 1507–1516.

[15] A.M. Carvajal-Bernal, F. Gómez, L. Giraldo, J.C. Moreno-Piraján, Adsorption of phenol and 2,4-dinitrophenol on activated carbons with surface modifications, Microporous Mesoporous Mater. 209 (2015) 150–156.

[16] G. Yang, H. Chen, H. Qin, Y. Feng, Amination of activated carbon for enhancing phenol adsorption: effect of nitrogen-containing functional groups, Appl. Surf. Sci. 293 (2014) 299–305.

[17] D.P. Vargas, L. Giraldo, J.C. Moreno-Piraján, Co(2) adsorption on activated carbon honeycomb-monoliths: a comparison of Langmuir and tóth models, Int. J. Mol. Sci. 13 (2012) 8388–8397.

[18] H.-P. Boehm, Chapter thirteen - surface chemical characterization of carbons from adsorption studies, in: E.J. Bottani, J.M.D. Tascón (Eds.), Adsorption by Carbons, Elsevier, Amsterdam, 2008, pp. 301–327.

[19] D.T. Cromer, J.B. Mann, X-ray scattering factors computed from numerical Hartree–Fock wave functions, Acta Crystallogr. - Sect. A Cryst. Phys. Diffr. Theor. Gen. Crystallogr. 24 (1968) 321–324.

[20] A. Sharma, T. Kyotani, A. Tomita, Comparison of structural parameters of pf carbon from xrd and hrtem techniques, Carbon 38 (2000) 1977–1984.

[21] W. Ruland, X-ray studies on the carbonization and graphitization of acenaphthylene and bifluorenyl, Carbon 2 (1965) 365–378.

[22] M. Shiraishi, K. Kobayashi, An x-ray study of coal tar pitch, Bull. Chem. Soc. Jpn. 46 (1973) 2575–2578.

[23] M. Dubinin, L. Radushkevich, Equation of the characteristic curve of activated charcoal, Chem. Zentr 1 (1947) 875.

[24] S. Brunauer, P.H. Emmett, E. Teller, Adsorption of gases in multimolecular layers, J. Am. Chem. Soc. 60 (1938) 309–319.

[25] D.D. Do, Adsorption analysis: equilibria and kinetics, Vol. 2, World Scientific, 1998.

[26] C. Moreno-Castilla, Adsorption of organic molecules from aqueous solutions on carbon materials, Carbon 42 (2004) 83–94.

[27] J. Figueiredo, M. Pereira, M. Freitas, J. Orfao, Modification of the surface chemistry of activated carbons, Carbon 37 (1999) 1379–1389.

https://doi.org/10.1016/j.heliyon.2019.e01156

[28] A. Cuesta, P. Dhamelincourt, J. Laureyns, A. Martinez-Alonso, J.D. Tascón, Raman microprobe studies on carbon materials, Carbon 32 (1994) 1523−1532.

[29] A. Lazzarini, A. Piovano, R. Pellegrini, G. Leofanti, G. Agostini, S. Rudić, M. Chierotti, R. Gobetto, A. Battiato, G. Spoto, A comprehensive approach to investigate the structural and surface properties of activated carbons and related pd-based catalysts, Catal. Sci. Technol. 6 (2016) 4910−4922.

[30] J.-S. Roh, Structural study of the activated carbon fiber using laser Raman spectroscopy, Carbon letters 9 (2008) 127−130.

[31] N. Shimodaira, A. Masui, Raman spectroscopic investigations of activated carbon materials, J. Appl. Phys. 92 (2002) 902−909.

[32] L. Lu, V. Sahajwalla, C. Kong, D. Harris, Quantitative x-ray diffraction analysis and its application to various coals, Carbon 39 (2001) 1821−1833.

[33] T.J. Bandosz, Activated Carbon Surfaces in Environmental Remediation, Vol. 7, Academic press, 2006.

[34] H. Marsh, F. Rodríguez-Reinoso, Chapter 1 - introduction to the scope of the text, in: Activated Carbon, Elsevier Science Ltd, Oxford, 2006, pp. 1−12.

[35] D.E. Sands, Introducción a la cristalografía, Reverté, 1993.

[36] O. Hamdaoui, E. Naffrechoux, Modeling of adsorption isotherms of phenol and chlorophenols onto granular activated carbon: Part i. Two-parameter models and equations allowing determination of thermodynamic parameters, J. Hazard Mater. 147 (2007) 381−394.

[37] J. McMurry, Química Orgánica. 7ª, Edición. Cengage Learning, 2008.

 https://doi.org/10.1016/j.heliyon.2019.e01156